KINETICS, CATALYSIS, AND REACTION ENGINEERING

Selective Catalytic Reduction of NO over Commercial DeNO$_x$ Catalysts: Comparison of the Measured and Calculated Performance

M. Koebel* and M. Elsener

Combustion Research, Paul Scherrer Institute, CH-5232 Villigen PSI, Switzerland

The performance of selective catalytic reduction monolithic catalysts may best be characterized by plotting the ammonia slip as a function of the percentage of NO_x conversion achieved. Experimental results obtained on a Diesel engine test stand have been compared with predicted values obtained by model calculations. In this way the possibilities and limits of such calculations could be shown. The model has no adjustable parameters. An exact prediction of performance is not possible under all conditions due to minor differences in composition between the real exhaust and the test gas mixtures used in the determination of the intrinsic catalyst properties. The value of such a model therefore lies in the prediction of the performance of new catalysts (e.g., layer catalysts) or under changed operating conditions (other temperature or GHSV).

Introduction

In a previous publication (Koebel and Elsener, 1998) we have outlined our general goal of developing and testing a model to evaluate the performance of selective catalytic reduction (SCR) catalytic reactors under stationary conditions. It is important to realize that in the practical application of the SCR DeNO$_x$ process the maximum possible NO_x conversion is not a useful value as it is achieved only at the expense of excessive ammonia slip: In practice only lower NO_x conversions may be attained, and their values are determined by the maximum permissible ammonia slip. The best way to characterize the performance of a SCR catalyst is therefore to plot the ammonia slip as a function of NO_x conversion at varying stoichiometry NH_3:NO (usually referred to as α).

The model is based on a number of publications on the subject (e.g., Buzanowski and Yang, 1990; Beeckman and Hegedus, 1991; Tronconi et al., 1992). In contrast to previous work we have determined experimentally all intrinsic properties of the examined catalysts; the model therefore has no adjustable parameters. The experimental determination of the intrinsic kinetics and of the thermodynamic adsorption parameters for the tested catalysts has been given in the above paper (Koebel and Elsener, 1998). The three catalysts are of the commercial SCR-DeNO$_x$ type and are composed mainly of TiO_2 (≈80%), WO_3 (≈9%), and V_2O_5 (1−3%). Catalyst D21 is a weakly active catalyst with ≈1% V_2O_5; catalysts D31 and D35 are medium active catalysts with ≈3% V_2O_5. Further details will be given below.

Early calculations had shown a strong dependence of the calculated catalyst performance on the values of the effective diffusion coefficients used. On the other hand, rather differing values of the effective diffusion coefficient were found in the literature (Buzanowski and Yang, 1990; Beeckman, 1991; Tronconi et al., 1992). We have therefore decided to measure the effective diffusion coefficient of NO in N_2 for some catalysts by the method described by Beeckman (1991). Before presenting the mathematical model and the results, we shall therefore report on the experimental determination of the effective diffusion coefficient.

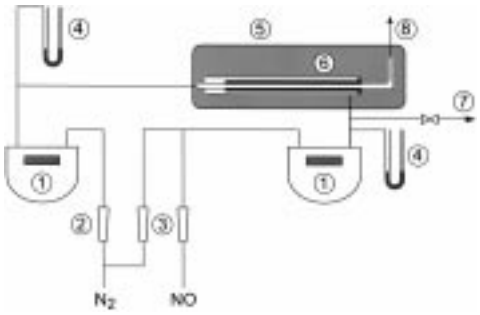

Figure 1. Experimental setup for measuring effective diffusion coefficients: 1, gas meter; 2, flowmeter for N_2; 3, flowmeter for NO/N_2; 4, pressure gauge; 5, furnace; 6, monolith in glass tube; 7, NO(in) measurement; 8, NO(out) measurement.

Measurement of the Effective Diffusion Coefficient

Figure 1 shows the experimental setup used in the diffusion experiments. The right end of a single monolithic channel of the catalyst sample is glued inside a larger glass tube (6). The ends of the monolithic channel are also glued to glass tubes matching the channel diameter using silicone rubber. In order to mix

* Author to whom correspondence is addressed. Telephone: +41-56-310 26 04. Fax: +41-56-310 21 99. E-mail: Manfred.Koebel@psi.ch.

S0888-5885(97)00569-1 CCC: $15.00
Published on Web 02/02/1998

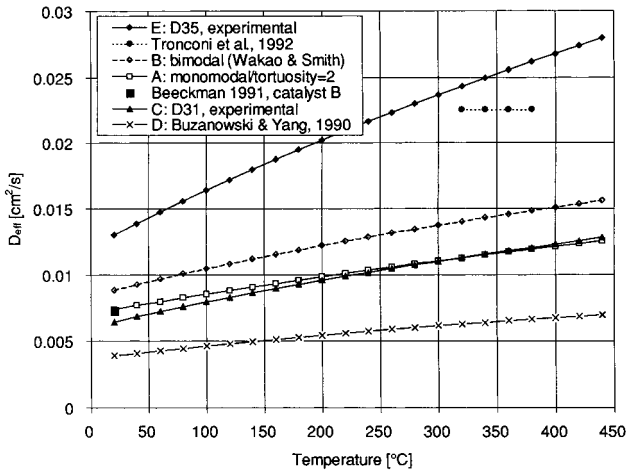

Figure 2. Diffusion coefficients as a function of temperature.

the effluent gas stream, a steel wire spiral is inserted into the right end of the glass tube. A further wire spiral between the monolith and large glass tube provided mixing of the incoming stream of NO in N_2. With the catalysts having 200 cpsi (cells per square inch), i.e., D31 and D35, the investigation of a single monolith channel was not possible; therefore, a section of 2 × 2 channels was used.

A mixture of about 1000 ppm NO in N_2 was fed to the outside and in countercurrent pure N_2 to the inside of the monolithic channel. In order to simplify the evaluation of the results, both gas streams were made equal within ±5% (≈200 L_N/h). The increase in NO concentration of the inside stream was monitored by a chemiluminescence analyzer (Eco Physics CLD 700 EL). Quasistationary measurements were made at about 20, 90, 160, and 220 °C. The equation given by Beeckman (1991) was used to evaluate the results:

$$\frac{1}{D_{\text{eff,NO}}} = \frac{1}{w}\left(\frac{c_1^{\text{in}} - c_2^{\text{out}}}{c_2^{\text{out}}}\frac{L\sigma}{V_2^*} - \frac{1}{k_{c1}} - \frac{1}{k_{c2}}\right) \qquad (1)$$

where L and σ are length and perimeter of the channel (σ refers to the inside of the channels), w is its wall thickness, V_2^* is the volumetric gas flow rate inside the channel, c_1^{in} is the inlet concentration of NO outside the channel (≈1000 ppm), and c_2^{out} the NO outlet concentration inside the channel (N_2 side). k_{c1} and k_{c2} are the mass-transfer coefficients on the gas side outside and inside the channel. They were assumed to be equal to k_{c2}, and this value was calculated using Hawthorn's equation (1974); as a result, their contribution to the total diffusion resistance amounted to up to 15%.

Figure 2 shows typical results of measured effective diffusion coefficients in comparison with calculated values. Three curves (A, B, C) lie close together. According to our experience most of the "standard" SCR catalysts lie in this region; this region seems to present the result of a pore size distribution of TiO_2 without special manufacturing procedures. The values taken from Buzanowski and Yang (1990) (curve D) seem to be definitely too low, and the experimental values for D35 (curve E) are almost 2 times higher than those of a catalyst with standard pore size distribution. According to its manufacturer, special measures were taken to enhance the amount of macropores.

The calculation "A" was made with the simple model assuming gas phase and Knudsen diffusion in a monomodal solid (Satterfield, 1980) and the following parameters typical for a SCR catalyst. This calculation contains the tortuosity, a factor not known exactly, and therefore does not allow a safe prediction of the effective diffusion coefficient:

$$\text{pore radius} = 1000 \text{ nm}$$

$$\text{porosity} = 0.555 \text{ cm}^3/\text{cm}^3$$

$$\text{BET} = 60 \text{ m}^2/\text{g}$$

$$\text{bulk density} = 1.85 \text{ cm}^3/\text{g}$$

$$\text{tortuosity} = 2.0$$

(recommended by Beeckman (1991))

The calculation "B" was made according to the model of Wakao and Smith (1962), a model that does not contain an adjustable factor and is therefore fully predictive. The following bimodal pore size distribution was used that corresponds to the measured values of D31:

$$\text{radius of mesopores} = 1400 \text{ nm}$$

$$\text{radius of macropores} = 10\,000 \text{ nm}$$

$$\text{porosity of mesopores} = 0.483 \text{ cm}^3/\text{cm}^3$$

$$\text{porosity of macropores} = 0.02 \text{ cm}^3/\text{cm}^3$$

Comparing the results with the experimental values obtained for catalyst D31 (curve C), we see that the model overestimates the real values of the diffusion coefficient up to about 35%, especially at low temperatures. The simple model calculation "A" fits the experimental values much better, but a value of the tortuosity must be assumed.

The values of $D_{\text{eff,NO}}$ (units: [cm²/s]) of three curves in Figure 2 in the temperature range 0−450 °C may be represented by the following equations:

Experiment, catalyst D35, "E":

$$D_{\text{eff,NO}} = 0.0019653T^{2.25}/(1285.9T^{0.5} + 1.529T^{1.75})$$

T in K

Experiment, catalyst D31, "C":

$$D_{\text{eff,NO}} = 0.00088935T^{2.25}/(905.24T^{0.5} + 1.61255T^{1.75})$$

T in K

Model calculation, "A":

$$D_{\text{eff,NO}} = 0.00082174T^{2.25}/(287.24T^{0.5} + 1.6807T^{1.75})$$

T in K

Mathematical Description of the Model

General Description. Figure 3 shows a section through the monolith. The flow direction of the gas is z, the opening of the (square) monolith cell is b, and the wall thickness is w. The catalyst length is divided into zz elements of height Δz and a material balance is made over each element. NO (and equimolar NH_3) enters the element at $\Delta z = 0$ and is partly consumed at the catalyst wall: NO flows from the gas bulk to the catalyst surface (x-direction). This flow is $\dot{n}_{\text{gas}}$, and the equal flow from the surface into the catalyst is $\dot{n}_{\text{solid}}$. The resulting

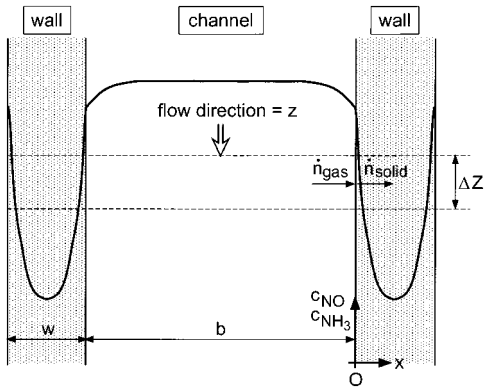

Figure 3. Section through a monolith.

concentration gradient on the gas side is given by the mass-transfer coefficient $k_{c,NO}$, the concentration gradient on the solid side by both diffusion and intrinsic kinetics of NO in the solid. The resulting decrease in concentration over the element Δz may then be calculated.

Simplifying Assumptions. The model considers (a) the mass transfer in the gas phase, (b) the intrinsic kinetics of NO with adsorbed NH_3, (c) the thermodynamics of NH_3 adsorption on the catalyst, and (d) the diffusion rates of NO and NH_3 in the catalyst pores.

The following effects are neglected:

(a) Temperature effects due to the exothermal reaction enthalpy ($\Delta T \approx 13$ K at 1000 ppm NO). The reaction conditions are therefore assumed to be isothermal.

(b) Deviations from ideal plug flow (axial dispersion).

(c) The influence of concentration variations of other components in the gas, especially O_2 and water. We note that the intrinsic kinetics determined in part 1 of this work (Koebel and Elsener, 1998) were measured in the presence of 5% water and 10% O_2, typical conditions of a Diesel engine exhaust gas.

(d) Possible side reactions due to the reaction of ammonia with oxygen or NO_x at high temperatures (formation of N_2O or NO_x).

(e) The effective diffusion coefficients of NO and NH_3 in the catalyst are assumed to be equal: $D_{eff,NO} = D_{eff,NH_3}$.

Mass-Transfer Resistance on the Gas Side. The mass-transfer coefficient $k_{c,NO}$ for NO may be obtained from the Sherwood number:

$$Sh = \frac{k_{c,NO} b}{D_{NO}} \tag{2}$$

A correlation for the local Sherwood number depending on the distance z from the catalyst entrance was used in the calculations (Tronconi et al., 1992):

$$Sh(z) = 2.977 + 8.827(1000z^*)^{-0.545} \exp\{-48.2z^*\} \tag{3}$$

$$z^* = \frac{zD_{NO}}{vb^2} = \frac{z/b}{(Re)(Sc)} \tag{4}$$

The characteristic Reynolds and Schmidt numbers are defined as

$$Re = vb/\nu \tag{5}$$

$$Sc = \nu/D_{NO} \tag{6}$$

Analogous equations exist for the mass transfer of ammonia; due to the slightly higher binary diffusion coefficient of ammonia, the corresponding value of k_{c,NH_3} is somewhat larger (by ≈10−20%). This difference is of negligible influence; therefore, in the calculations k_{c,NH_3} was assumed to be equal to $k_{c,NO}$.

Mass Transport and Reaction in the *x*-Direction. For a short channel element of length = Δz the mass balance of NO in the catalyst wall perpendicular to the flow direction is assumed to be constant and is given by

$$D_{eff,NO} \frac{d^2 c_{NO}}{dx^2} = \rho_{Cat} r_{NO} \tag{7}$$

The boundary conditions are

(a) at the interface gas/catalyst ($x =$ 0, superscript 0):

$$c_{NO} = c^0_{NO} \qquad \text{at } x = 0 \tag{8}$$

(b) in the middle of the catalyst wall ($x = h = w/2$):

$$\frac{dc_{NO}}{dx} = 0 \qquad \text{at } x = h \tag{9}$$

An equal set of equations describe the mass balance of ammonia:

$$D_{eff,NH_3} \frac{d^2 c_{NH_3}}{dx^2} = \rho_{Cat} r_{NO} \tag{10}$$

$$c_{NH_3} = c^0_{NO_3} \qquad \text{at } x = 0 \tag{11}$$

$$\frac{dc_{NH_3}}{dx} = 0 \qquad \text{at } x = 0 \tag{12}$$

Integrating (7) and (10) and equalizing yields

$$D_{eff,NO}(c^0_{NO} - c_{NO}) = D_{eff,NH_3}(c^0_{NH_3} - c_{NH_3}) \tag{13}$$

For the reaction rate the various rate laws discussed in the earlier publication (Koebel and Elsener, 1998) may be used. For example, in the case of a simple first-order law in NO and ammonia adsorption the rate equation is

$$r_{NO} = k_1 c_{NO} \frac{K_{NH_3} c_{NH_3}}{1 + K_{NH_3} c_{NH_3}} \tag{14}$$

The rate constants and adsorption constants are given by Arrhenius type equations:

$$k_1 = A \exp\left\{\frac{-E_A}{RT}\right\} \tag{15}$$

$$K_{NH_3} = K_{NH_3,0} \exp\left\{\frac{-H_{ad,NH_3}}{RT}\right\} \tag{16}$$

Due to the 1:1 stoichiometry of the SCR reaction, the fluxes of NO and NH_3 through the gas film are equal

Table 1. Test-Stand Measuring Conditions

	D21		D31		D35	
approx. power [$kW_{el.}$]	T [°C]	GHSV [h^{-1}]	T [°C]	GHSV [h^{-1}]	T [°C]	GHSV [h^{-1}]
100	455	24 000	455	32 200	455	30 300
75	400	20 000	400	28 900	405	26 400
50	325	17 000	330	25 300	335	22 900
40	285	16 000	295	24 400	295	21 700
30	250	15 300	255	23 200	255	20 500
25	230	14 900	235	22 600	235	20 200

and yield

$$k_{c,NO}(c_{NO}^{bulk} - c_{NO}^{0}) = k_{c,NH_3}(c_{NH_3}^{bulk} - c_{NH3}^{0}) \qquad (17)$$

As mentioned above equal values of $k_{c,NO}$ and k_{c,NH_3} were used in the calculation; this leads to a further simplification of (17).

A further condition is given by the equality of fluxes on the gas and the catalyst side:

$$k_{c,NO}(c_{NO}^{bulk} - c_{NO}^{0}) = D_{eff,NO}\left(\frac{dc_{NO}}{dx}\right)_0 \qquad (18)$$

Mass Balance over the Volume Element of Length Δz. If the volumetric flow in the channel is V^* and the length of the element is Δz, the mass balance for NO over the element is

$$V^* c_{NO}^{in} = V^*(c_{NO}^{in} + \Delta c_{NO}) + \Delta z \sigma k_{c,NO}(c_{NO}^{in} - c_{NO}^{0}) \qquad (19)$$

σ is the inside perimeter of the channel. The decrease in NO concentration over the element of length Δz is

$$\Delta c_{NO} = -\frac{1}{V^*}(\Delta z \sigma k_{c,NO}(c_{NO}^{in} - c_{NO}^{0})) \qquad (20)$$

An equal mass balance is valid for ammonia. The equations were solved numerically. The number of knots in the z-direction was 50. In the x-direction the number of knots varied between 50 and 200; the larger values proved to be necessary for the fast catalysts D31 and D35 at higher temperatures, where the concentration gradient in the catalyst gets very steep at the interface.

Further Assumptions

All three catalysts were evaluated on a Diesel engine test stand. The engine is a 6-cylinder, 4-stroke, direct-injection, turbocharged Diesel engine with intercooler (MAN D 0826 LE) running at fixed 1500 rpm. Details of the test stand have been given previously (Koebel et al., 1996). The average catalyst temperatures and space velocities (humid, 1013 mbar, 0 °C) of the six points measured are given in Table 1. The three catalysts are further characterized by the properties given in Table 2.

The exhaust gas coming from the Diesel engine contains ≈2000 ppm NO_x at the maximum load (100 $kW_{el.}$) and ≈1000 ppm at the minimum load (25 $kW_{el.}$); the exact concentrations of NO_x(in) were used in the calculations. The fraction of NO_2 is about 10% of NO_x over the whole range; its positive effect on the SCR kinetics was neglected.

Table 3 summarizes some of the kinetic parameters obtained in the earlier work (Koebel and Elsener, 1998) and used in the model calculations. These parameters

Table 2. Properties of the Three Catalysts

property	units	D21	D31	D35
cell density	cells/in.^{2}	100	200	200
opening b	mm	2.14	1.37	1.4
wall thickness w	mm	0.4	0.4	0.37
BET	m^2/kg	60000	54000	45000
bulk density	kg/m^3	1850	1780	1520
channel length	m	0.4	0.3	0.25
$D_{eff,NO}$ used for calculation	m^2/s	"D31"	"D31"	"D35"

Table 3. Arrhenius Parameters Assuming First-Order Reaction ($n = 1$)

catalyst	exp. no.	NO_{in} [ppm]	A [$cm^3/(g·s)(mol/cm^3)^{1-n}$]	E_A [kJ/mol]
D21	V8	1000	7.45×10^9	85.9
D21	V10	70	5.48×10^8	69.8
D31	V1	1000	1.02×10^{10}	77.2
D35	V10	1000	1.46×10^{10}	78.1

Table 4. Arrhenius Parameters of Ammonia and NO Adsorption

parameter	units	value	catalyst
$K_{NH3,0}$	Pa^{-1}	3.0×10^{-12}	D21
$H_{ad,NH3}$	J/mol	−137000	D21
$K_{NO,0}$	Pa^{-1}	5.02×10^{-5}	D35
$H_{ad,NO}$	J/mol	−21300	D35
$k_{NO,0}$	mol/(g·s)	333	D35
$E_{A,NO}$	J/mol	74700	D35

are valid for first-order reaction in NO. As shown in the above work, the reaction rate would be higher at lower concentrations and low temperatures: this effect is neglected in the calculations using the kinetic expression with $n = 1$.

Finally we compile the thermodynamic adsorption parameters of ammonia and nitric oxide in Table 4. This table also contains the parameters $k_{NO,0}$ and $E_{A,NO}$ that describe the kinetics assuming NO adsorption.

Results

Some Basic Cases. Figure 4 shows the profiles along a 200 cpsi catalyst of DeNO$_x$ (NO_x reduction), ϕ_{NH_3} (at the surface), and the concentrations of NH_3 in the gas bulk and on the catalyst surface at GHSV = 25 000 h^{-1} and $\alpha = 1.0$ for 450 °C (Figure 4a) and 250 °C (Figure 4b). In the calculation the kinetics of D21/V8/$n = 1$ were assumed. Due to the assumption of $\alpha = 1.0$ the concentrations of NH_3 shown also represent those of NO.

450 °C: The maximum ammonia adsorption ϕ_{NH_3} of ≈65% is found directly at the catalyst entrance; it then decreases steadily due to falling ammonia concentration to reach a value of only ≈8% at the catalyst outlet. These values of ϕ_{NH_3} show that the reaction rate is strongly reduced at 450 °C due to a low coverage of active NH_3. It is also interesting to look at the concentrations of NH_3 (or NO) in the bulk and at the surface: At the entrance the values are 1000 and ≈800 ppm. This shows that about 20% of the total "reaction resistance" is due to the limited mass transfer on the gas side; the rest of this resistance is due to limited diffusion and reaction rate within the catalyst. On the other hand, at the catalyst outlet the mass-transfer resistance on the gas side is practically negligible because the reaction rate within the catalyst has diminished so strongly (low concentrations of NO and NH_3 and small ϕ_{NH_3}). It is

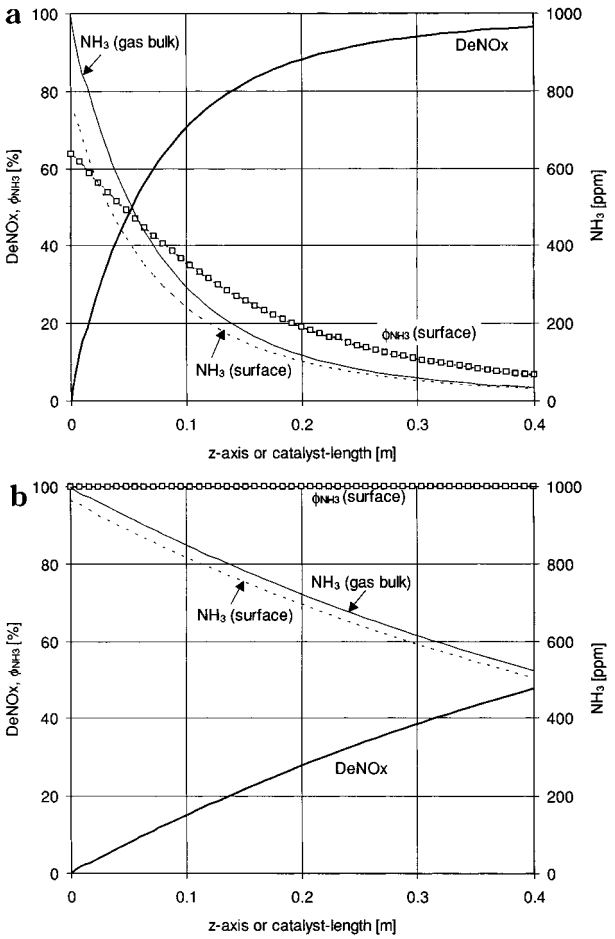

Figure 4. Profiles of $DeNO_x$, NH_3/NO concentration, and ϕ_{NH_3} along a catalyst. 200 cpsi, GHSV = 25 000 h^{-1}, $\alpha = 1.0$, NO(in) = 1000 ppm, kinetics D21/V8/n = 1. (a) T = 450 °C. (b) T = 250 °C.

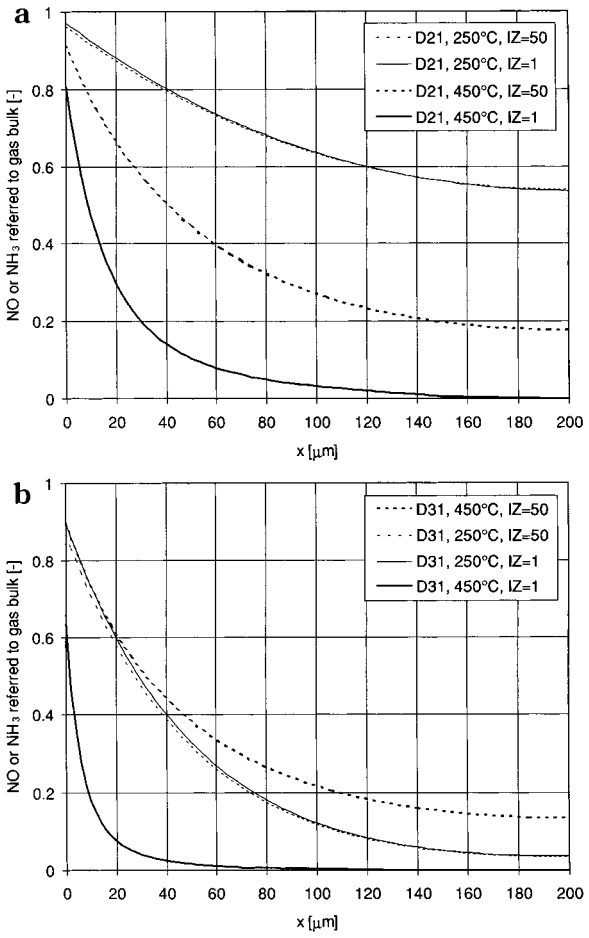

Figure 5. Profiles of NH_3/NO in catalyst wall at entrance (IZ = 1) and end (IZ = 50). 200 cpsi, GHSV = 25 000 h^{-1}, $\alpha = 1.0$, NO(in) = 1000 ppm. (a) Kinetics D21/V8/n = 1. (b) Kinetics D31/V1/n = 1.

also evident that the $DeNO_x$ only increases modestly by doubling the catalyst length from 0.2 to 0.4 m.

250 °C: At lower temperatures, ϕ_{NH_3} remains always at 100%. This is due partly to the much higher value of K_{ad,NH_3} but also to the higher NH_3 concentrations linked to a $DeNO_x$ of only ≈50% at the catalyst end. The latter is due mainly to the lower reaction rate at this temperature and reflects itself also in a small concentration difference of NH_3(gas bulk) − NH_3(surface).

In Figure 5 we show the relative concentration profiles of NH_3 (or NO) within the catalyst wall (x-direction) under the same conditions at the entrance (channel element number 1) and the outlet (channel element number 50). The calculations are shown for the slow catalyst D21 (Figure 5a) and the fast catalyst D31 (Figure 5b).

D21: At 450 °C and IZ = 1, the relative concentration drops rapidly from ≈80% to ≈4% at 100 μm ($^1/_4$ of wall thickness), which shows a high diffusion resistance and therefore a relatively low internal effectiveness of the catalyst. At 450 °C and IZ = 50 the relative concentration drops from about 90% to only ≈20% in the middle of the wall: at these conditions the internal effectiveness of the catalyst is already much better. A definitely better internal effectiveness is observed at 250 °C: here also the deeper layers contribute clearly to the performance of the catalyst, and the concentration profiles are practically the same at the entrance and at the outlet.

D31: The faster kinetics lead to a lower internal effectiveness of the catalyst. Compared with D21, the reaction resistance in the catalyst is lower, with the resistance of mass transfer on the gas side being about the same. Therefore, at 450 °C at the catalyst entrance, the relative concentration at the interface is lower and falls clearly faster than with D21. The two concentration profiles (IZ = 1 and 50) at 250 °C are again identical and fall much more rapidly than with D21 due to the faster kinetics of D31.

It may therefore be concluded that at higher temperatures only a thin layer of the catalyst wall is used, whereas at lower temperatures and especially with slow catalysts the whole wall thickness contributes to the performance of the catalyst. In Figure 6 we have compared the performance of a plain, extruded catalyst (wall thickness again 400 μm) with a coated catalyst having a layer thickness of 35 μm. The graph shows the ammonia slip as a function of the corresponding NO conversion for three temperatures and is obtained by varying the stoichiometric ratio α. It may be seen that, at temperatures of 300 °C and above, the layer catalyst behaves practically as well as the extruded catalyst. Only the curves at 250 °C show a significant advantage for the extruded catalyst containing more mass. With a catalyst showing slower kinetics or lower values of D_{eff}, the performance of the layer catalyst would fall off already at higher temperatures.

Catalyst D21. Figure 7a shows experimental results obtained on the Diesel engine test stand at six operating

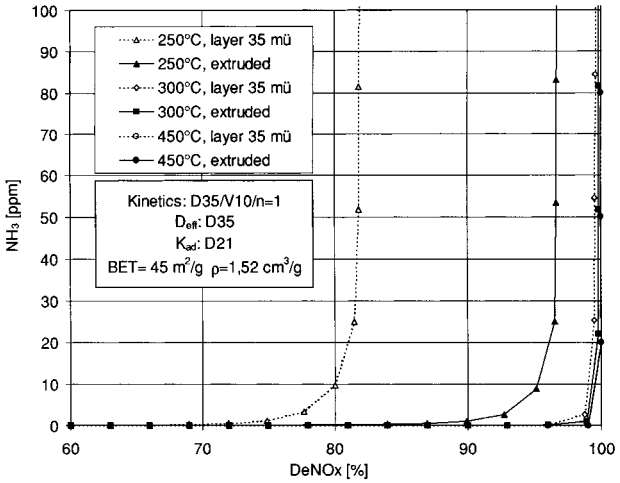

Figure 6. Comparison for an extruded and a layer catalyst. 200 cpsi, GHSV = 25 000 h^{-1}; varying α, NO(in) = 1000 ppm, kinetics D35/V10/n = 1.

points. Parts b and c of Figure 7 show the corresponding calculated results using two different kinetic expressions:

(a) In Figure 7b the rate expression of D21/V8 was used, i.e., $n = 1$ at NO(in) = 1000 ppm.

(b) In Figure 7c a rate expression considering NO adsorption was used. This was obtained from the Arrhenius parameters for k_1 at 70 ppm NO(in), i.e., D21/V10 and of the NO adsorption constant for D35.

It can be seen that both calculations describe the real behavior qualitatively correctly. Especially, the abnormal behavior of the series 455 °C, 24 000 h^{-1}, is shown in both calculations: Up to a temperature of 400 °C the performance increases with temperature. But the curve at 455 °C starts to rise already at quite low values of $DeNO_x$. Therefore, a given ammonia slip of, e.g., 10 ppm allows a lower $DeNO_x$ at 450 °C than at 400 °C or even 325 °C. This effect is due to the decreasing adsorption constant of ammonia, K_{ad,NH_3}. An influence from beginning ammonia oxidation may be ruled out as the rate constant of ammonia oxidation is about a factor 500 smaller than of the SCR reaction (Koebel and Elsener, 1998). None of the calculated figures can really match the experimental curves exactly. The calculation in Figure 7c, where NO adsorption was considered, probably comes nearest to reality. Especially at lower temperatures these curves show a better performance and therefore agree better with experimental values.

In a plot $NH_3 = f(DeNO_x)$ generally two values of NO_x conversion are of interest:

(a) The maximum possible $DeNO_x$ at a very high NH_3 slip. At low and intermediate temperatures this value corresponds to the maximum ammonia coverage of the catalyst ($\phi_{NH_3} = 1$) but cannot be used in the technical application of SCR. At high temperatures, i.e., above ≈400 °C, $\phi_{NH_3} = 1$ will no longer be fulfilled and therefore the maximum $DeNO_x$ will fall off.

(b) A value of $DeNO_x$ at an NH_3 slip which is tolerable in practice, e.g., 10 ppm. Depending on the type of catalyst and operating conditions, this value may be much lower than the maximum possible $DeNO_x$.

Catalyst D31. Figure 8a shows the experimental results obtained on the Diesel engine test stand. Although the space velocities are higher, the performance of the catalyst at comparable temperatures is much better than that of D21. This is mainly due to its higher intrinsic activity.

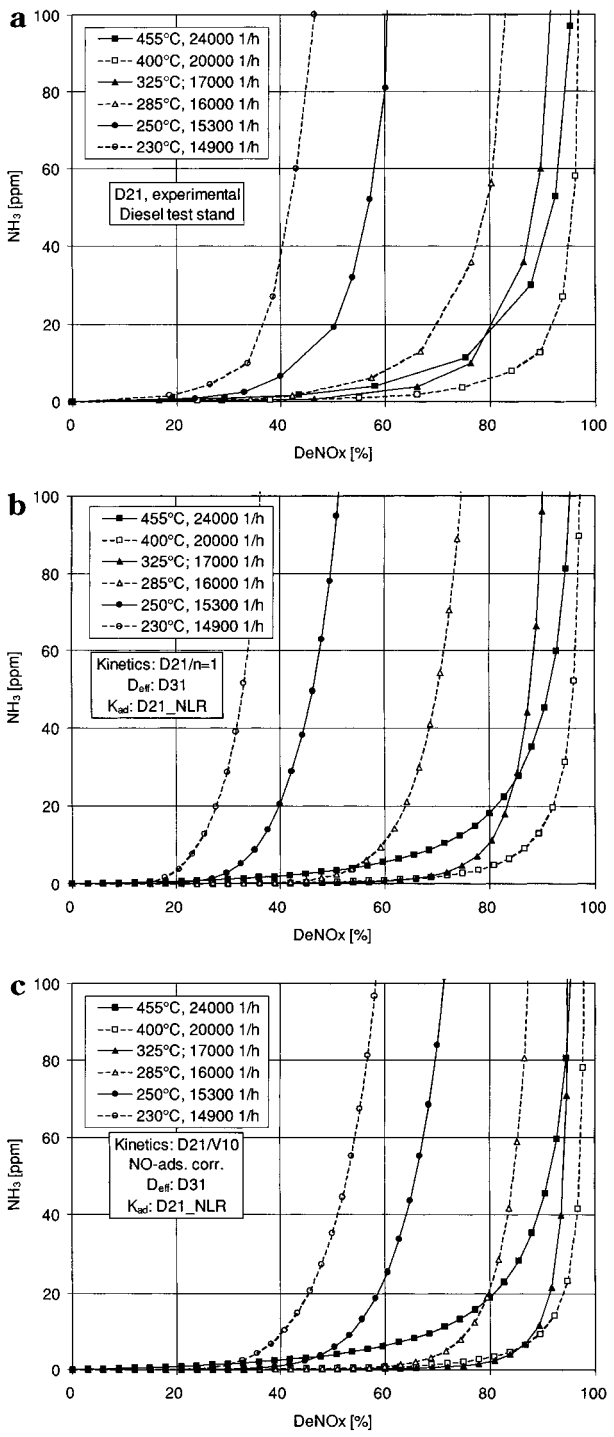

Figure 7. Catalyst D21: Ammonia slip as a function of $DeNO_x$. (a) Experimental results obtained on the Diesel test stand. (b) Calculated results for the Diesel test stand. Kinetics D21/V8/n = 1. (c) Calculated results for the Diesel test stand. Kinetics D21/V10 considering NO adsorption.

Figure 8b shows calculated results using the simple first-order rate law. It is evident that the calculated curves suggest a better catalyst performance than reality, and this is especially pronounced at temperatures below 330 °C. Further calculations using a kinetic law considering NO adsorption (rate and adsorption laws as determined for D35) are not shown but give similar results.

Catalyst D35. Figure 9a shows the experimental results obtained on the Diesel engine test stand. At comparable space velocities, the performance of the

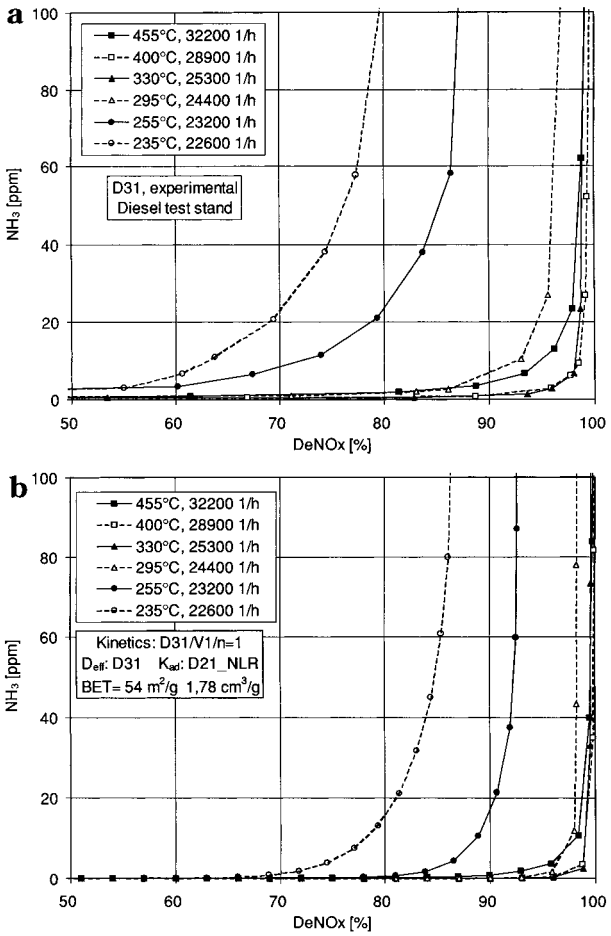

Figure 8. Catalyst D31: Ammonia slip as a function of $DeNO_x$. (a) Experimental results obtained on the Diesel test stand. (b) Calculated results for the Diesel test stand. Kinetics D31/V1/n = 1.

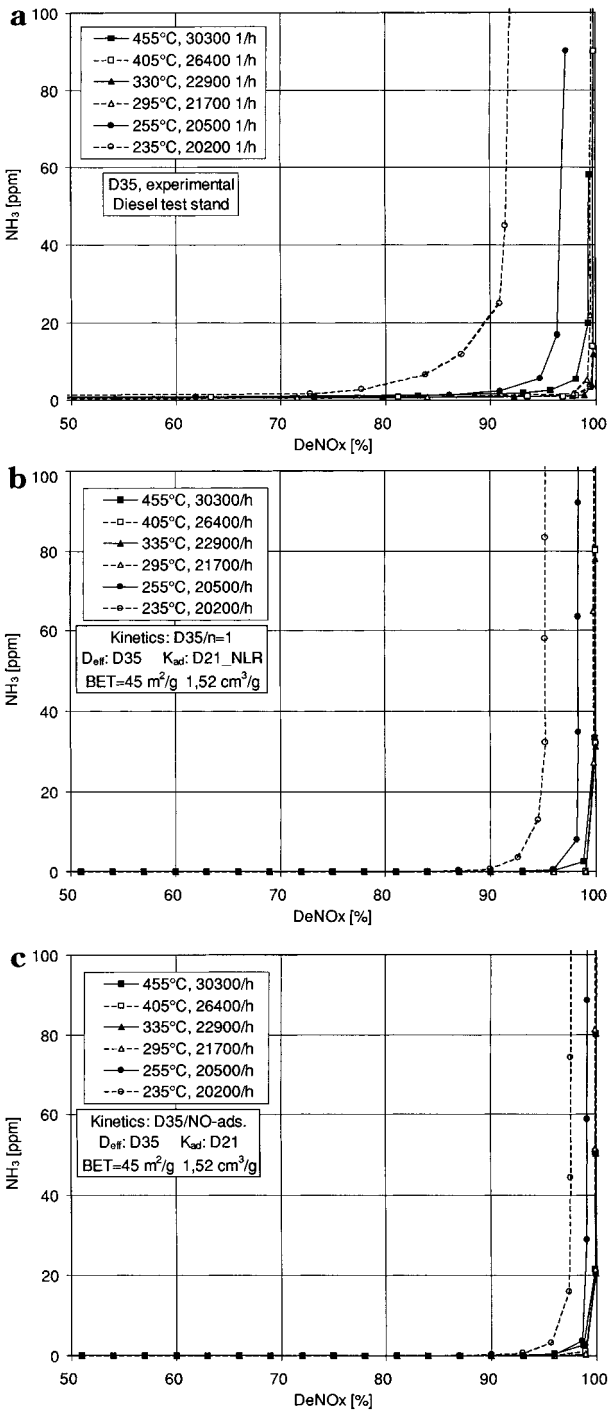

Figure 9. Catalyst D35: Ammonia slip as a function of $DeNO_x$. (a) Experimental results obtained on the Diesel test stand. (b) Calculated results for the Diesel test stand. Kinetics D35/V10/n = 1. (c) Calculated results for the Diesel test stand. Kinetics D35 considering NO adsorption.

catalyst is still better than D31. The intrinsic rate constants of the two catalysts being similar, this is due to the higher effective diffusion coefficient of D35. This catalyst also shows steeply rising ammonia slip when approaching the maximum $DeNO_x$; therefore, the difference between maximum $DeNO_x$ and $DeNO_x$ at 10 ppm NH_3 is much smaller than with D21 or D31. This shows that this catalyst is sized generously in terms of activity.

Parts b and c of Figure 9 show the calculations using the first-order rate law and considering NO adsorption. As in the case of D31, the calculated curves suggest a better catalyst performance than that observed in the experiment. The general observation with these two higher-activity catalysts ($\approx$3% V_2O_5) therefore was that the calculated values overestimated their real SCR performance, especially at low temperatures.

In view of these observations we have searched for a possible reason. We determined the kinetic parameters on powdered samples in the same way as described in the previous publication (Koebel and Elsener, 1998), but using a side stream of real exhaust gas coming from the Diesel engine. Much lower rate constants were found in this way. When these were used in the model calculation, the NH_3-DeNO_x curves were displaced to the left; i.e., at a given $DeNO_x$ the ammonia slip was much higher. The curves showed a catalyst performance even worse than reality. This proves that gas components in the Diesel exhaust depress the activity of the catalyst, with this being especially pronounced at lower temperatures.

Discussion

The model can basically describe the performance of a SCR monolithic reactor, i.e., its behavior NH_3 slip vs $DeNO_x$. However, it has also been shown that fully quantitative predictions are not possible, especially for the more active catalysts D31 and D35 and at higher space velocities.

We see several reasons for these discrepancies:

(a) The determination of the parameters is usually made in a simulated gas composition not containing typical components of the real exhaust gas. In the case of Diesel exhaust an inhibition due to other components (probably hydrocarbons) could clearly be shown, especially at lower temperatures. An opposite effect may be caused by the NO_2 fraction contained in Diesel exhaust: It is a well-known fact that an equimolar mixture of NO + NO_2 has a higher reaction rate than NO alone (Ramis et al., 1990).

(b) Kinetic and thermodynamic parameters: The experimentally determined kinetic and thermodynamic parameters generally contain a high level of uncertainty: It should be remembered that the *kinetic parameters* must usually be extrapolated from quite low temperatures (200−275 °C) to much higher temperatures (up to 450 °C) or are obtained by applying an internal effectiveness factor not known exactly. The *adsorption parameters* can rarely all be measured experimentally for every catalyst due to the time involved and sometimes due to experimental constraints (e.g., K_{NH_3} cannot be determined for a very active catalyst). We have therefore assumed that the values determined for one catalyst may be transferred to the others: We have always used K_{NH_3} determined for D21, and K_{NO} determined for D35. The assumption of a pure Langmuir adsorption isotherm is another simplification which will lead to errors in the evaluation of adsorption parameters.

(c) We have shown in the first part of this publication that a kinetic expression considering NO adsorption represents the intrinsic kinetics better than a simple first-order rate law. However, in the present calculations, only the performance of D21 could be simulated better by this kinetic expression; in the case of D35 the simple first-order rate law gave better agreement. The uncertainties discussed above therefore remain a deciding factor. The use of a more sophisticated kinetic expression than a simple first-order rate law supplemented by ammonia adsorption is therefore hardly justified in model calculations.

(d) Finally also the effective diffusion coefficients cannot be determined exactly, especially for fine channel geometries exceeding ≈ 32 cpsi. D31 and D35 have 200 cpsi, and the uncertainties in the diffusion coefficients are estimated to ±20%.

In conclusion the present model is a valuable tool in predicting semiquantitatively the performance of new catalysts and especially the influence of certain parameters such as effective diffusion coefficient, intrinsic kinetics, monolith structure, or GHSV. A good example is the prediction of the performance of a layer catalyst shown above. On the other hand, an *exact* prediction of the performance (x % $DeNO_x$ at 10 ppm NH_3 slip) under realistic conditions does not appear possible at present.

Clearly a much better correspondence between experimental and calculated behavior could be obtained if at least one of the important parameters would be fitted, as it is the usual practice when such models are used. However, the goal of this work was to base the calculations fully on experimentally determined parameters.

Acknowledgment

The financial support of the Swiss Federal Office of Energy (BEW) is gratefully acknowledged.

List of Symbols

A = preexponential factor [$cm^3/(g·s)$]
b = channel opening [m]
c = concentration [mol/m^3]
D_{NO} = binary diffusion coefficient NO/N_2 [m^2/s]
$D_{eff,i}$ = effective diffusion coefficient of NO or NH_3 in catalyst
E_A = activation energy [J/(mol·K)]
H_{ad} = adsorption enthalpy [J/(mol·K)]
h = catalyst layer thickness [m]
k_1 = first-order rate constant [$m^3/(kg·s)$]
k_c = mass-transfer coefficient [m/s]
K = adsorption equilibrium constant [1/Pa] or [m^3/mol]
L = channel length [m]
r = reaction rate [mol/(kg·s)]
R = gas constant [8.314 J/(mol·K)]
T = temperature [K]
v = gas velocity [m/s]
V^* = volumetric gas flow [m^3/s]
w = wall thickness [m]
x = direction perpendicular to gas flow
X_{NO} = conversion of NO ("$DeNO_x$")
z = direction of gas flow

Greek Symbols
α = stoichiometric ratio NH_3:NO
η_{Cat} = internal effectiveness factor ("catalyst efficiency")
ϑ = temperature [°C]
ν = kinematic viscosity [m^2/s]
ρ_{Cat} = bulk catalyst density [kg/m^3]
σ = perimeter of channel (=4b)
ϕ = relative adsorption

Subscripts
NH_3 = ammonia
NO = NO
0 = preexponential

Subscripts
in = at catalyst entrance
out = after catalyst
bulk = in gas bulk
0 = at the interface

Literature Cited

Beeckman, J. W. Measurement of the Effective Diffusion Coefficient of Nitrogen Monoxide through porous Monolith-Type Ceramic Catalysts. *Ind. Eng. Chem. Res.* **1991**, *30*, 428.

Beeckman, J. W.; Hegedus, L. L. Design of Monolith Catalysts for Power Plant NOx Emission Control. *Ind. Eng. Chem. Res.* **1991**, *30*, 969.

Buzanowski, M. A.; Yang, R. T. Simple Design of Monolith Reactor for Selective Catalytic Reduction of NO for Power Plant Emission Control. *Ind. Eng. Chem. Res.* **1990**, *29*, 2074.

Hawthorn, R. D. Afterburner Catalysts, Effects of Heat and Mass Transfer between Gas and Catalyst Surface. *AIChE Symp. Ser.* **1974**, *137*, 428.

Koebel, M.; Elsener, M. Selective Catalytic Reduction of NO over Commercial DeNOx-Catalysts: Experimental Determination of Kinetic and Thermodynamic Parameters. *Chem. Eng. Sci.* **1998**, in press.

Koebel, M.; Elsener, M.; Marti, T. NOx-Reduction in Diesel Exhaust Gas with Urea and Selective Catalytic Reduction. *Combust. Sci. Technol.* **1996**, *121* (1−6) p 67.

Ramis, G.; Busca, G.; Bregani, F.; Forzatti, P. Fourier Transform Infrared Study of the Adsorption and Coadsorption of Nitric Oxide, Nitrogen Dioxide and Ammonia on Vanadia−Titania and Mechanism of Selective Catalytic Reduction. *Appl. Catal.* **1990**, *64*, 259.

Satterfield, C. N. *Heterogeneous Catalysis in Practice;* McGraw-Hill Book Co.: New York, 1980.

Tronconi, E.; Forzatti, P.; Gomez Martin, J. P.; Malloggi, S. Selective Catalytic Removal of NOx: A Mathematical Model for Design of Catalyst and Reactor. *Chem. Eng. Sci.* **1992**, *47*, 2401.

Wakao, N.; Smith, J. M. Diffusion in Catalyst Pellets. *Chem. Eng. Sci.* **1962**, *17*, 825.

Received for review August 18, 1997
Revised manuscript received November 11, 1997
Accepted November 25, 1997

IE970569H